The Astrophysical Journal, 945:17 (6pp), 2023 March 1 https://doi.org/10.3847/1538-4357/acba0d

Repeating Emission Episodes in Gamma-Ray Bursts: Millilensing or Jet Precession?

He Gao[1,2], An Li[2], Wei-Hua Lei[3], and Zhi-Qiang You[2,4]
[1] Institute for Frontier in Astronomy and Astrophysics, Beijing Normal University, Beijing 100875, People's Republic of China; gaohe@bnu.edu.cn
[2] Department of Astronomy, Beijing Normal University, Beijing 100875, People's Republic of China
[3] Department of Astronomy, School of Physics, Huazhong University of Science and Technology, Wuhan, Hubei 430074, People's Republic of China
[4] Advanced Institute of Natural Sciences, Beijing Normal University, Zhuhai 519087, People's Republic of China
Received 2022 September 18; revised 2023 February 1; accepted 2023 February 6; published 2023 March 2

Abstract

Recently, some gamma-ray bursts (GRBs) whose light curves consist of repeating emission episodes with similar temporal profiles have attracted extensive attention. They are proposed to be candidates of millilensing events, although smoking gun evidence is lacking, since there are no redshift measurements and no angular offset detections for any of these candidates. Here we show that without invoking gravitational lensing, the repeating light-curve properties of these GRBs could also be interpreted under the jet precession model, as long as the detectable period in every precession circle is less than the precession period, and the precession period is close to the jet emission duration. By fitting the gamma-ray light curves of these GRBs, we suggest that the jet precession angle for these bursts should be relatively small (e.g., $\theta_p < 5\overset{\circ}{.}3$), and the jet structure for these bursts are more likely Gaussian. The results suggest us to be careful when identifying millilensing GRBs. Multiband afterglow data and especially angular offset detections are essential to provide comprehensive justification for this identification.

Unified Astronomy Thesaurus concepts: Gamma-ray bursts (629)

1. Introduction

Most recently, the search for gravitational lensing effects in gamma-ray bursts (GRBs) has attracted extensive attention. Searches for macrolensing events (i.e., independently triggered GRB pairs with similar light curves and spectra) have yielded null results (Nemiroff & Wickramasinghe 1994; Veres et al. 2009; Davidson et al. 2011; Li & Li 2014; Hurley et al. 2019; Ahlgren & Larsson 2020). However, several candidates of millilensing events (i.e., two emission episodes in a single triggered GRB with similar light-curve patterns and similar spectral properties) have been proposed. For instance, Paynter et al. (2021) claimed the identification of a possible gravitationally lensed burst, GRB 950830, via Bayesian analysis of the BATSE light-curve data set, and the inferred lens mass, depending on the unknown lens redshift, falls into the mass range of intermediate-mass black holes (BHs; e.g., $\sim 10^4$–$10^5\,M_\odot$). Later, Wang et al. (2021) and Yang et al. (2021) claimed that GRB 200716C is also a possible gravitationally lensed GRB, with a possible lens mass of about $\sim 10^5\,M_\odot$ in the rest frame. Veres et al. (2021) claimed that GRB 210812A contains signatures of a million solar mass gravitational lens. Lin et al. (2022) presented a systematic search for millilensing of GRBs in data from Fermi-GBM, and more interesting candidates (GRB 081126A, GRB 090717A, GRB 081122A, and GRB 110517B) were proposed.

If these candidates truly are lensed events, they could serve as promising cosmological and astrophysical probes (see Oguri 2019 for a review). For instance, they can be used to derive constraints on the abundance of compact dark matter in the mass range 10^4–$10^7\,M_\odot$ (i.e., intermediate-mass BHs; Paynter et al. 2021; Veres et al. 2021; Wang et al. 2021; Yang et al. 2021; Lin et al. 2022). Difference of time delays between multiple images among different energy channels could be used for testing fundamental physics from the propagation speed (Biesiada & Piórkowska 2009; Collett & Bacon 2017; Fan et al. 2017; Lan et al. 2022). Unfortunately, however, there are no redshift measurements and no angular offset detections for any of these candidates, making it rather difficult to determine whether they are really gravitational lens events.

One interesting question is "Without invoking lensing effects, is there any physical model that could make two (or even more) emission episodes in a single triggered GRB with similar light-curve patterns and similar spectral properties?"

When a GRB is powered by a hyperaccreting process of a debris torus surrounding a spinning BH, the misalignment in the spin axis of the BH and the angular momentum axis of the BH–disk system, if it exists, could drive the accretion disk to precess by the Lense–Thirring torque, which is known as Lense–Thirring precession (Lense & Thirring 1918). In this case, the ultrarelativistic jet launched from the central engine, driven either by neutrino annihilation or the Blandford–Znajek mechanism, would also be precessing (Lei et al. 2007; Liu et al. 2010; Liu & Xue 2012). It has long been discussed that the global profile of a GRB light curve, as well as the spectral evolution, may be modulated by jet precession (Blackman et al. 1996; Fargion 1999; Portegies Zwart et al. 1999; Portegies Zwart & Totani 2001; Fargion & Grossi 2006; Lei et al. 2007; Liu et al. 2010; Liu & Xue 2012; Wang et al. 2022).

In this work, we first briefly revisit the jet precession model and investigate how variant combinations of the precession angle (θ_p), jet opening angle (θ_j), and observation angle ($\theta_{\rm obs}$) affect the light-curve behaviors of GRBs. And then we show that with proper parameter combinations, the jet precession model could well interpret those GRBs that contain two (or even more) similar emission episodes. Our results suggest to us to be careful when identifying millilensing GRBs. Multiband afterglow data and especially angular offset detections are essential to provide comprehensive justification of such an

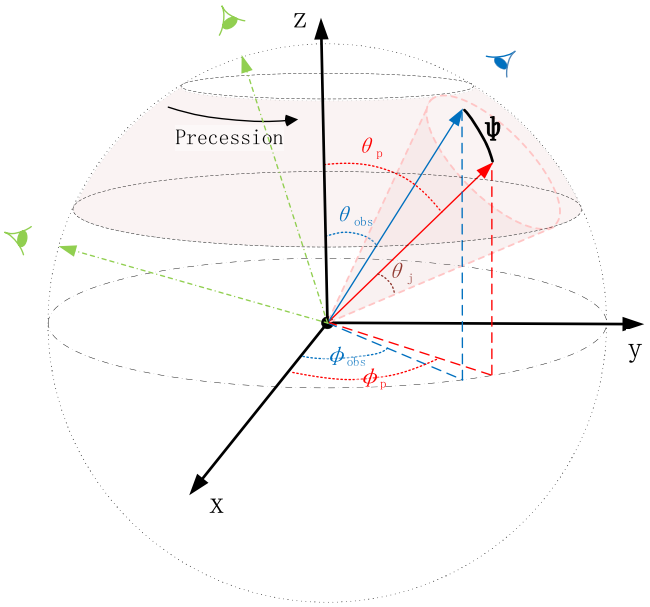

Figure 1. Schematic picture of a precessing jet.

identification (Huang & Liu 2021; Chen et al. 2022; Huang & Liu 2022).

2. Jet Precession Model

After decades of study, two types of progenitors were invoked for GRBs, i.e., core collapse from Wolf–Rayet stars for LGRBs (Woosley 1993; Paczyński 1998; MacFadyen & Woosley 1999; Woosley & Bloom 2006) and mergers of two compact stellar objects (neutron star–neutron star, NS–NS, and NS–BH systems) for SGRBs (Paczynski 1986; Eichler et al. 1989; Paczynski 1991; Narayan et al. 1992). After the catastrophic destruction of the progenitor system, a central engine must form to power a relativistic jet. Here we consider a hyperaccreting BH as the central engine. The anisotropic fallback mass in the collapsar model or the different directions of the angular momenta of the two compact objects may impart precession between the BH and accretion disk due to the Lense–Thirring torque. In this case, the ultrarelativistic jet launched from the central engine, driven either by neutrino annihilation or the Blandford–Znajek mechanism, would also be precessing (Lei et al. 2007; Liu et al. 2010; Liu & Xue 2012; Wang et al. 2022).

A schematic picture of a precessing jet could be described in spherical coordinates (see Figure 1). The jet is precessing around the zenith with precession angle θ_p. The jet opening angle is θ_j. The line of sight between the observer and the total momentum of the BH + disk is fixed as ($\theta_{\rm obs}$, $\phi_{\rm obs}$). The angle between the observer and the central locus of the jet is

$$\Psi(t) = \cos^{-1}[\cos\theta_p\cos\theta_{\rm obs} + \sin\theta_p\sin\theta_{\rm obs}\cos(\phi_p(t) - \phi_{\rm obs})], \quad (1)$$

where $\phi_p(t) = 2\pi t/P$ is the azimuth angle of the jet and P is the precession period.

Due to the beaming effect, γ-ray photons are detectable only when $\Psi(t) \lesssim \theta_j + 1/\Gamma$, where Γ is the Lorenz factor of the jet. In principle, when $\Psi(t)$ is slightly larger than θ_j, jet radiation is still detectable but the flux would quickly drop off due to the beaming effect. Off-beam radiation would behave as a small segment of exponential rise and decay at the bottom of each emission episode, which is normally negligible considering the typically large velocities of GRB jets. For the purpose of this paper, here we only consider on-beam situations, i.e., $\Psi \lesssim \theta_j + 1/\Gamma$ when $\phi_p = \phi_{\rm obs}$ (observers marked with blue instead of green in Figure 1). In this case, the detectable period in every precession circle could be estimated as

$$\Delta T = \frac{P}{\pi}\cos^{-1}\left[\frac{\cos\theta_j - \cos\theta_{\rm obs}\cos\theta_p}{\sin\theta_{\rm obs}\sin\theta_p}\right]. \quad (2)$$

Within each detectable period, the observed luminosity will be regulated by two aspects; one is the luminosity distribution in the jet as a function of the distance to the central locus ($f(\theta)$), and the other is the temporal evolution of the jet emission (represented by the temporal profile of the luminosity at the central locus $L_0(t)$), i.e.,

$$L(t) = L_0(t) f(\theta = \Psi(t)). \quad (3)$$

In the literature, various models have been invoked for the luminosity distribution within the jet:

1. Gaussian distribution (Zhang & Mészáros 2002)

$$f(\theta) = e^{-\frac{\theta^2}{2\theta_c^2}}, \quad (4)$$

for $\theta < \theta_w$, where θ_c is the characteristic angle of the core and θ_w is the truncating angle of the jet.

2. Power-law distribution (Mészáros et al. 1998; Rossi et al. 2002)

$$f(\theta) = \begin{cases} 1, & \theta < \theta_0, \\ (\theta/\theta_0)^{-k}, & \theta \geqslant \theta_0, \end{cases} \quad (5)$$

when $\theta > \theta_0$, the angular peak luminosity decreases as a power law.

3. Gaussian distribution + cocoon (Bromberg et al. 2011)

$$f(\theta) = e^{-\frac{\theta^2}{2\theta_{c,1}^2}} + \eta e^{-\frac{\theta^2}{2\theta_{c,2}^2}}. \quad (6)$$

Two Gaussian components are involved in this model: a narrower, brighter jet defined by L_0 and $\theta_{c,1}$ and a wider, fainter cocoon defined by ηL_0 and $\theta_{c,2}$.

The overall profile of the gamma-ray light curve essentially depends on the relations between P (the precession period), ΔT (the detectable period in every precession circle), and $T_{\rm dur}$ (the total duration of jet emission). Some examples for different cases are shown in Figure 2. When $\Delta T \ll P \ll T_{\rm dur}$ (Figure 2(a)), multiple pulses with width ΔT would show up at intervals of $P - \Delta T$. When $\Delta T \sim P \ll T_{\rm dur}$ (Figure 2(b)), multiple pulses with width P would show up without any intervals. For these two cases, the shape of an individual pulse is essentially determined by the jet structure, i.e., the luminosity distribution in the jet as a function of the distance to the central locus. When the energy distribution in the jet is uniform or axisymmetric, the shape of the observed pulse tends to be symmetric. Otherwise, if the energy distribution in the jet is highly asymmetric, the pulse shape will be asymmetric and be related to the direction of jet precession. It may rise faster or decay faster, depending on whether the part with higher energy or the part with lower energy in the jet enters the line of sight first. The envelope line of these multiple pulses reflects the temporal evolution of $L_0(t)$.

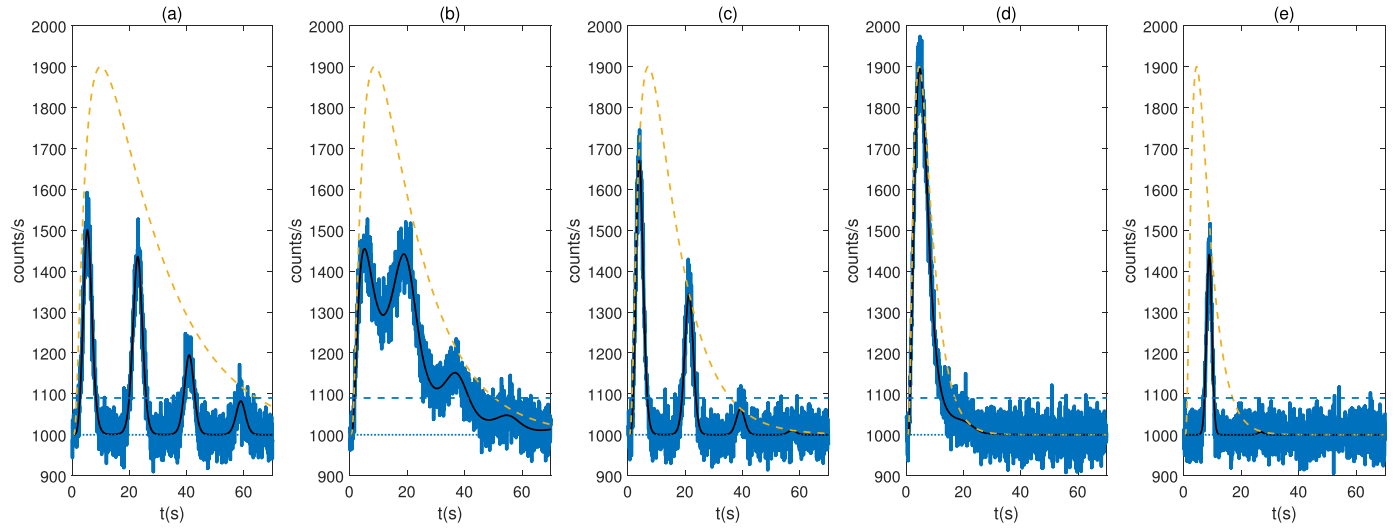

Figure 2. Example light curves for different situations: (a) $\Delta T \ll P \ll T_{\rm dur}$, (b) $\Delta T \sim P \ll T_{\rm dur}$, (c) $\Delta T \ll P \lesssim T_{\rm dur}$, (d) $\Delta T \sim P \sim T_{\rm dur}$, and (e) $P > T_{\rm dur}$. The orange dashed lines reflect the temporal evolution of the jet emission, the blue dotted lines mark the simulated background, and the blue dashed lines mark the detection threshold. When simulating the light curves, we adopt a Gaussian jet structure and add Poisson noise.

On the other hand, when $\Delta T \ll P \lesssim T_{\rm dur}$ (Figure 2(c)), two pulses with similar temporal profiles may appear. In special situations (e.g., $2\Delta T + P > T_{\rm dur}$), the second pulse may be shorter than the first one (or even disappear). In this case, the shapes of both pulses are also determined by the jet structure. When $\Delta T \sim P \sim T_{\rm dur}$ (Figure 2(d)), the light curve only consists of one pulse with width P, whose temporal profile is related to the temporal evolution of $L_0(t)$. Finally, when $P > T_{\rm dur}$ (Figure 2(e)), only one pulse with width ΔT is expected, whose temporal profile is determined by the jet structure function instead of the evolution of $L_0(t)$. For these three situations, no periodic signal is expected.

The temporal evolution of $L_0(t)$ is rather difficult to predict, since it is related to many factors, including the central engine activities, the dissipation process of the jet, and the radiation mechanism. From an observational point of view, many single-pulse GRBs with an asymmetric exponential-rise, exponential-decay (FRED) profile have been detected (Norris et al. 1996, 2005; Shao et al. 2017), but for many observed multipulsed GRBs, the envelope shapes of the multiple peaks are complex and irregular, indicating that the temporal evolution of $L_0(t)$ may have strong individuality. In order to generate the examples in Figure 2, here we assume the temporal evolution of the jet emission follows the FRED shape as

$$L_0(t) = \begin{cases} A e^{-\left(\frac{|t-t_{\rm max}|}{\sigma_r}\right)^{\nu}}, & t < t_{\rm max}, \\ A e^{-\left(\frac{|t-t_{\rm max}|}{\sigma_d}\right)^{\nu}}, & t > t_{\rm max}, \end{cases} \quad (7)$$

where A is the normalization parameter, $t_{\rm max}$ is the peak time, σ_r and σ_d are the rise and decay time constants, respectively, and ν measures the sharpness of the pulse.

3. Model Application

So far, seven GRBs have been proposed to contain two emission episodes with similar light-curve patterns: one is detected by BATSE (GRB 950830) and the others are all detected by Fermi-GBM (GRB 081122A, GRB 081126A, GRB 090717A, GRB 110517B, GRB 200716C, and GRB 210812A). For the purpose of this work, we download the observed data of GRB 950830 from the online database.[5] We use light curves with 64 ms resolution obtained by BATSE in the four Large Area Detector energy channels, 20–300 keV. We download the data of the other bursts from the Fermi Science Support Center's FTP site.[6] Here we adopt NaI with the highest signal-to-noise ratio (S/N) and use its time-tagged event data that records each photon's arrival time with 2 μs temporal resolution, as well as information regarding in which eight of the 128 energy channels the photon registered. The light curves of these seven GRBs are extracted and plotted in Figure 3.

For each of the seven GRBs, we use Gaussian, power-law, and Gaussian + cocoon models to fit its individual emission episodes. A Gaussian likelihood is applied for parameter estimation and model selection by nested sampling in `dynesty` (Higson et al. 2019). We apply the logarithm of the Bayes factor (BF) to perform the model selection between model M_1 and model M_2 by $\ln {\rm BF}^1_2 = \ln \mathcal{Z}_1(d|M_1) / \mathcal{Z}_2(d|M_2)$, where the $\mathcal{Z}$ is the evidence of model M, which is the integration of the product of the likelihood and priors to the parameters. The logarithm of BF for the fittings are collected in Table 1. We find that the Gaussian model is strongly supported when compared with the power-law model since almost all the $\ln({\rm BF}^{\rm G}_{\rm PL})$ values are larger than 2. Also, we find anecdotal evidence to support the Gaussian model compared with the Gaussian + cocoon model, since $\ln({\rm BF}^{\rm G}_{\rm G+c})$ is in range of [0, 1.1] (Andraszewicz et al. 2015). According to the fitting results, if these GRBs are indeed from precessing jets, their jet structures are likely Gaussian.

In Figure 4, we plot how $\Delta T/P$ varies with different combinations of θ_p and θ_j. Here we show three situations when $\theta_{\rm obs} = \frac{1}{2}\theta_p$ (Figure 4(a)), $\theta_{\rm obs} = \theta_p$ (Figure 4(b)), and $\theta_{\rm obs} = 2\,\theta_p$ (Figure 4(c)). It is obvious that for a given θ_p, the larger θ_j is, the closer ΔT is to P. Taking the width of the first episode as ΔT and the intervals between the starting points of two episodes as P, we plot the $\Delta T/P$ for the seven candidate GRBs

[5] http://heasarc.gsfc.nasa.gov/docs/cgro/batse/
[6] http://heasarc.gsfc.nasa.gov/FTP/fermi/data/gbm/bursts/

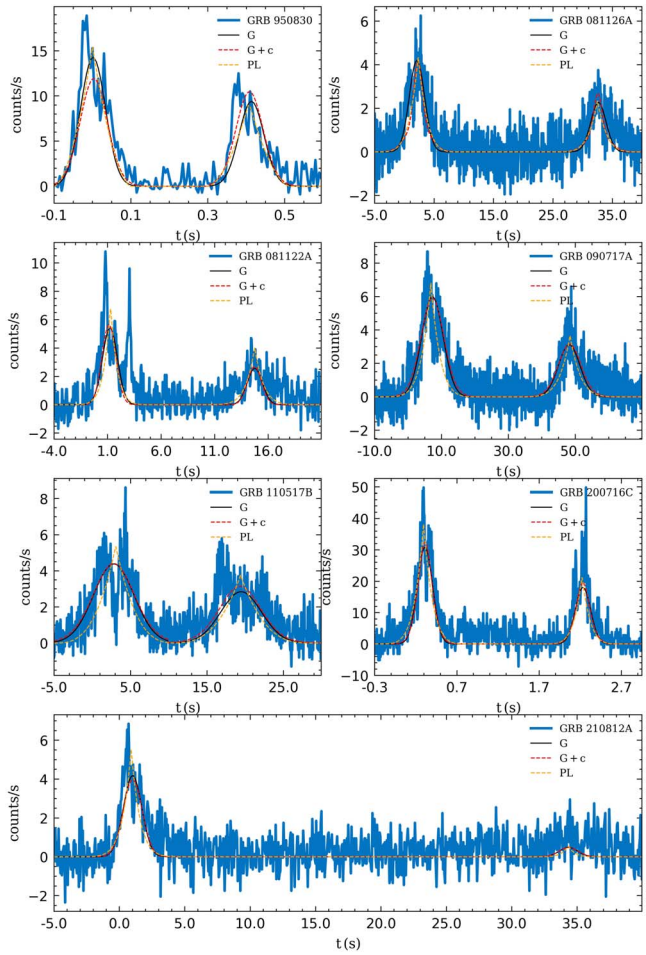

Figure 3. Light curves of the GRB candidates with repeating emission episodes. The best-fitting results for the Gaussian, Gaussian + cocoon, and power-law models are shown as the black solid lines, red dashed lines, and orange dashed lines, respectively.

in Figure 4. We find that for a typical jet opening angle,[7] all of the $\Delta T/P$ values could be well interpreted by the precession model as long as the precession angle θ_p is not too large. For each candidate, the upper limit of θ_p is presented in Table 1. Among these bursts, GRB 210812A may have the largest precession angle (e.g., $\theta_p < 5.^\circ3$ for the $\theta_{\rm obs} = \theta_p$ case, $\theta_p < 4.^\circ2$ for the $\theta_{\rm obs} = \frac{1}{2}\theta_p$ case, and $\theta_p < 2.^\circ1$ for the $\theta_{\rm obs} = 2\,\theta_p$ case). It is worth noting that a small precession angle is in line with the theoretical expectation, since (1) the anisotropic fallback mass cannot produce a large angle between the BH and the fallback mass in collapsars, and (2) the merger process of a compact binary may reduce the misalignment between the angular momenta of the two compact objects (Liu et al. 2010).

4. Conclusion and Discussion

Recently, some interesting GRBs have attracted extended attention, whose light curves consist of multiple emission episodes with similar temporal profiles. These GRBs are proposed to be candidates of millilensing events, but smoking gun evidence is lacking, since there are no redshift measurements and no angular offset detections for any of these candidates. Here we show that, alternatively, the special light-curve properties of these GRBs could be due to the jet precession effect instead of gravitational lensing effect. If our interpretation is correct, the following implications can be inferred:

1. A certain fraction of GRBs may be powered by precessing jets. When the detectable period in every precession circle (ΔT) is less than the precession period (P), and the precession period is close to the jet emission duration, GRBs produced by precessing jets would consist of two (or even more) emission episodes with similar temporal profiles.
2. For an individual emission episode, the pulse shape essentially reflects the jet structure, i.e., the luminosity distribution in the jet as a function of the distance to the central locus. When the energy distribution in the jet is uniform or axisymmetric, the shape of the observed pulse tends to be symmetric, which is insensitive to the direction from which the jet originated. On the other hand, if the energy distribution in the jet is highly asymmetric, the pulse shape will be asymmetric and be related to the direction of jet precession. It may rise faster or decay faster, depending on whether the part with the higher energy or the part with the lower energy in the jet enters the line of sight first. It is interesting to note that for the current candidates adopted in this work, their pulse shapes are relatively symmetrical, inferring that the energy distributions of the jets that power these bursts are relatively symmetrical. Nevertheless, it is found that a Gaussian jet structure is more favorable than a power-law structure or a Gaussian + cocoon structure.
3. According to the ratio between ΔT and P, for a typical jet opening angle, the jet precession angle should be small. GRB 210812A may have the largest precession angle, $\theta_p < 5.^\circ3$ for the $\theta_{\rm obs} = \theta_p$ case, $\theta_p < 4.^\circ2$ for the $\theta_{\rm obs} = \frac{1}{2}\theta_p$ case, and $\theta_p < 2.^\circ1$ for the $\theta_{\rm obs} = 2\,\theta_p$ case.

In addition to their similar temporal behaviors, the emission episodes included in some proposed candidates also show certain similar spectral properties (Veres et al. 2021; Lin et al. 2022, for details), which is expected within the jet precession model. In a structured jet, the spectral properties would change with the viewing angle. For instance, in order to incorporate the observations of GRB 170817A with historical SGRB statistical data, Ioka & Nakamura (2019) found that the profile whereby E_p changes with the viewing angle θ should be $E_p(\theta) = E_{p,0} \times (1 + \theta/\theta_c)^{-0.4}$, where $E_{p,0}$ and the central luminosity of the Gaussian jet satisfy the Yonetoku relation (Yonetoku et al. 2004). In this case, the multiple emission episodes produced by the jet precession effect will naturally have a similar spectral behavior. It is worth noting that some discrepancies exist between the two emission episodes in some of our adopted double-peaked GRBs. For instance, with the so-called "χ^2 test" for testing the light-curve similarity of two episodes, Mukherjee & Nemiroff (2021a) argued that the light curves of two pulses in GRB 090717 differ at about the 5σ confidence level. Mukherjee & Nemiroff (2021b) found cumulative hardness discrepancies between the two pulses in GRB 950830 and thus argued that the case for GRB 950830 involving a gravitational lens may well be considered intriguing but should not be considered proven. The differences between the two pulses pose a certain challenge to the lensing

[7] From a systematic study of the jet breaks of Swift GRBs, the typical jet opening angle is found to be $(2.5 \pm 1)^\circ$ (Wang et al. 2018).

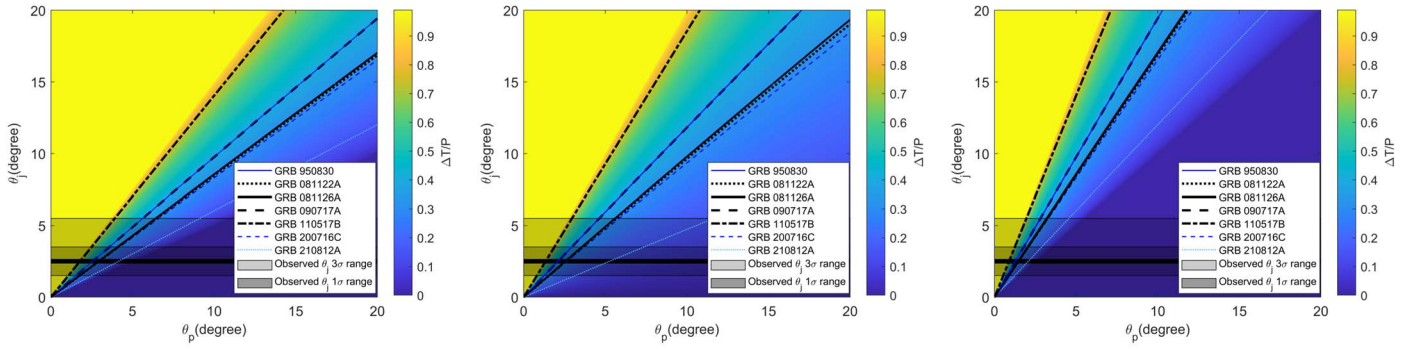

Figure 4. Contour plot of $\Delta T/P$ for different relationships between θ_p and θ_o: (a) $\theta_{\rm obs} = \frac{1}{2}\theta_p$, (b) $\theta_{\rm obs} = \theta_p$, and (c) $\theta_{\rm obs} = 2\,\theta_p$. The solid, dashed, and dotted lines mark the value of $\Delta T/P$ for the proposed candidates. The horizontal gray shadow stripes present the observed distribution of the jet opening angle.

Table 1
The BFs and θ_p Upper Limits

GRB Name	BF		θ_p Limit (°)		
	ln (BF^{G}_{G+c})	ln (BF^{G}_{PL})	$\theta_o = \theta_p/2$	$\theta_o = \theta_p$	$\theta_o = 2\,\theta_p$
GRB 950830	1.2	2.1	2.6	2.1	1.3
GRB 081122A	0.3	5.9	3.0	2.6	1.5
GRB 081126A	0.9	2.6	2.9	2.5	1.5
GRB 090717A	0.2	11.5	2.6	2.1	1.3
GRB 110517B	0.5	9.3	1.8	1.4	0.9
GRB 200716C	0.7	7.8	3.0	2.7	1.5
GRB 210812A	0.6	4.3	4.2	5.3	2.1

model. But in the jet precession model, certain discrepancies between different pulses are expected, since the jet always experiences expansion and energy dissipation in between it deviating and entering the direction of line of sight due to precession.

Considering the contamination of the jet precession effect, one needs to be careful when identifying millilensing GRBs. Multiband afterglow data are essential to provide comprehensive justification. In the lensing scenario, when different lensed images cannot be resolved, their signals would be superimposed together with a given time delay. In this case, the X-ray afterglows are likely to contain several X-ray flares of similar widths in linear scale and similar spectra, and the optical afterglow light curve will show sharp rebrightening signatures (Chen et al. 2022). While in the jet precession scenario, it is expected that peculiar polarization features in early optical afterglows (Huang & Liu 2022) and special energy injection signatures in X-ray/optical afterglows (Huang & Liu 2021) will be observed .

Lin et al. (2022) performed a systemic search among ∼3000 GRBs, and only four GRBs are found to consist of multiple similar emission episodes. Within the jet precession framework, such a low event rate (∼4/3000) is reasonable, since in order to show an obvious precession effect, the precession angle should be large relative to the jet opening angle, which requires that the misalignment in the spin axis of the BH and the angular momentum axis of the BH–disk system is large enough. For Type I GRBs (compact star merger origin), it is required that the angular momentum directions of the two compact stars are very different from the orbital angular momentum direction; for Type II GRBs (massive star origin), it is required that the angular momentum direction of the inner core region of the massive star is misaligned with the angular momentum direction of the outer fallback material. Specific numerical simulations are required in the future to investigate the chance of GRB engine precession, both for collapsars and compact object mergers. On the other hand, it is interesting that we only find candidates with two similar episodes instead of multiple quasiperiodic episodes. Nevertheless, periodicity is not an observed characteristic for most multipulsed GRBs (e.g., Dichiara et al. 2013). Such a fact might indicate that for most precessing GRB jets, the radiation timescale is somehow comparable to the precession period, which may provide clues for further revealing the nature and generation mechanism of precession jets.

We thank the anonymous referee for helpful comments that have helped us to improve the presentation of the paper. This work is supported by the National Natural Science Foundation of China (Projects 12021003, U2038107, and U1931203). We acknowledge the science research grants from the China Manned Space Project with Nos. CMS-CSST-2021-A13 and CMS-CSST-2021-B11.

Software: Fermi-GBM Data Tools (v1.1.1; Goldstein et al. 2022), bilby (Ashton et al. 2019). The data and code that support the findings of this study are available from the corresponding author upon request.

ORCID iDs

He Gao https://orcid.org/0000-0002-3100-6558
Wei-Hua Lei https://orcid.org/0000-0003-3440-1526

References

Ahlgren, B., & Larsson, J. 2020, ApJ, 897, 178

Andraszewicz, S., Scheibehenne, B., Rieskamp, J., et al. 2015, J. Manage., 41, 521
Ashton, G., Hübner, M., Lasky, P. D., et al. 2019, ApJS, 241, 27
Biesiada, M., & Piórkowska, A. 2009, MNRAS, 396, 946
Blackman, E. G., Yi, I., & Field, G. B. 1996, ApJL, 473, L79
Bromberg, O., Nakar, E., Piran, T., et al. 2011, ApJ, 740, 100
Chen, S., Wen, X., Gao, H., et al. 2022, ApJ, 924, 49
Collett, T. E., & Bacon, D. 2017, PhRvL, 118, 091101
Davidson, R., Bhat, P. N., & Li, G. 2011, in AIP Conf. Proc. 1358, Gamma-Ray Bursts, ed. J. E. McEnery, J. L. Racusin, & N. Gehrels (Melville, NY: AIP), 17
Dichiara, S., Guidorzi, C., Frontera, F., et al. 2013, ApJ, 777, 132
Eichler, D., Livio, M., Piran, T., et al. 1989, Natur, 340, 126
Fan, X.-L., Liao, K., Biesiada, M., et al. 2017, PhRvL, 118, 091102
Fargion, D. 1999, A&AS, 138, 507
Fargion, D., & Grossi, M. 2006, ChJAS, 6, 342
Goldstein, A., Cleveland, W., & Kocevski, D. 2022, Fermi GBM Data Tools: v1.1.1, https://fermi.gsfc.nasa.gov/ssc/data/analysis/gbm
Higson, E., Handley, W., Hobson, M., et al. 2019, Stat. Comput., 29, 891
Huang, B.-Q., & Liu, T. 2021, ApJ, 916, 71
Huang, B.-Q., & Liu, T. 2022, ApJ, 933, 103
Hurley, K., Tsvetkova, A. E., Svinkin, D. S., et al. 2019, ApJ, 871, 121
Ioka, K., & Nakamura, T. 2019, MNRAS, 487, 4884
Lan, L., Piórkowska-Kurpas, A., Wen, X., et al. 2022, ApJ, 937, 62
Lei, W. H., Wang, D. X., Gong, B. P., et al. 2007, A&A, 468, 563
Lense, J., & Thirring, H. 1918, PhyZ, 19, 156
Li, C., & Li, L. 2014, SCPMA, 57, 1592
Lin, S.-J., Li, A., Gao, H., et al. 2022, ApJ, 931, 4
Liu, T., Liang, E.-W., Gu, W.-M., et al. 2010, A&A, 516, A16
Liu, T., & Xue, L. 2012, ChPhB, 21, 069801
MacFadyen, A. I., & Woosley, S. E. 1999, ApJ, 524, 262
Mészáros, P., Rees, M. J., & Wijers, R. A. M. J. 1998, ApJ, 499, 301
Mukherjee, O., & Nemiroff, R. J. 2021a, RNAAS, 5, 183
Mukherjee, O., & Nemiroff, R. J. 2021b, RNAAS, 5, 103
Narayan, R., Paczynski, B., & Piran, T. 1992, ApJL, 395, L83
Nemiroff, R. J., & Wickramasinghe, W. A. D. T. 1994, ApJL, 424, L21
Norris, J. P., Bonnell, J. T., Kazanas, D., et al. 2005, ApJ, 627, 324
Norris, J. P., Nemiroff, R. J., Bonnell, J. T., et al. 1996, ApJ, 459, 393
Oguri, M. 2019, RPPh, 82, 126901
Paczynski, B. 1986, ApJL, 308, L43
Paczynski, B. 1991, AcA, 41, 257
Paczyński, B. 1998, ApJL, 494, L45
Paynter, J., Webster, R., & Thrane, E. 2021, NatAs, 5, 560
Portegies Zwart, S. F., Lee, C.-H., & Lee, H. K. 1999, ApJ, 520, 666
Portegies Zwart, S. F., & Totani, T. 2001, MNRAS, 328, 951
Rossi, E., Lazzati, D., & Rees, M. J. 2002, MNRAS, 332, 945
Shao, L., Zhang, B.-B., Wang, F.-R., et al. 2017, ApJ, 844, 126
Veres, P., Bagoly, Z., Horvath, I., et al. 2009, arXiv:0912.3928
Veres, P., Bhat, N., Fraija, N., et al. 2021, ApJL, 921, L30
Wang, X.-G., Zhang, B., Liang, E.-W., et al. 2018, ApJ, 859, 160
Wang, X.-I., Zhang, B.-B., & Lei, W.-H. 2022, ApJL, 931, L2
Wang, Y., Jiang, L.-Y., Li, C.-K., et al. 2021, ApJL, 918, L34
Woosley, S. E. 1993, ApJ, 405, 273
Woosley, S. E., & Bloom, J. S. 2006, ARA&A, 44, 507
Yang, X., Lü, H.-J., Yuan, H.-Y., et al. 2021, ApJL, 921, L29
Yonetoku, D., Murakami, T., Nakamura, T., et al. 2004, ApJ, 609, 935
Zhang, B., & Mészáros, P. 2002, ApJ, 571, 876